PHYSICS

Bell correlations between light and vibration at ambient conditions

Santiago Tarrago Velez[1], Vivishek Sudhir[2,3], Nicolas Sangouard[4,5]*, Christophe Galland[1]*

Time-resolved Raman spectroscopy techniques offer various ways to study the dynamics of molecular vibrations in liquids or gases and optical phonons in crystals. While these techniques give access to the coherence time of the vibrational modes, they are not able to reveal the fragile quantum correlations that are spontaneously created between light and vibration during the Raman interaction. Here, we present a scheme leveraging universal properties of spontaneous Raman scattering to demonstrate Bell correlations between light and a collective molecular vibration. We measure the decay of these hybrid photon-phonon Bell correlations with sub-picosecond time resolution and find that they survive over several hundred oscillations at ambient conditions. Our method offers a universal approach to generate entanglement between light and molecular vibrations. Moreover, our results pave the way for the study of quantum correlations in more complex solid-state and molecular systems in their natural state.

INTRODUCTION

In the hierarchy of nonclassical states, the Bell correlated states represent an extreme. When two parties share such a state, information can be encoded exclusively in the quantum correlations of the random outcomes of measurements between them (*1*, *2*). The strength of such correlations is quantified by Bell inequalities, whose violation demarcates Bell correlated states from less entangled ones (*3*).

Experimental realizations of Bell correlated states—whether between polarization states of light (*4*, *5*), individual atomic systems (*6*–*8*), in atomic ensembles (*9*–*11*), superconducting ciruits (*12*, *13*), or solid-state spins (*14*, *15*)—call for isolated systems that strongly interact with a well-characterized probe. Even mesoscopic acoustic resonators have been engineered to exhibit Bell correlations (*16*) thanks to long coherence times (achieved at milli-kelvin temperatures) and strong interaction with light (by integration with an optical microcavity).

Recent experiments have shown that high-frequency vibrations of bulk crystals (*17*–*22*) or molecular ensembles (*23*–*25*) can mediate nonclassical intensity correlations between inelastically scattered photons under ambient conditions (i.e., at room temperature and atmospheric pressure). In the pioneering work of Lee *et al.* (*17*), two phonon modes in spatially separated bulk diamonds had been entangled with each other by performing coincidence measurements and postselection on the Raman-scattered photons. Recently, leveraging a new two-tone pump-probe method (*22*), it became possible to follow the birth and death of an individual quantum of vibrational energy (i.e., Fock state) excited in a single spatiotemporal mode of vibration in a bulk crystal (*26*).

These experiments did not necessitate specially engineered subjects; they reveal fundamental quantum properties of naturally occurring materials. Together, these developments raise new questions: Are the correlations spontaneously created between light and vibration during Raman scattering strong enough to violate Bell inequalities?

How is the vibrational coherence time reflected in the dynamics of the hybrid light-vibration quantum correlations?

In this study, we demonstrate Bell correlations arising from the Raman interaction between light and mechanical vibration at ambient conditions and use them to resolve the decoherence of the vibrational mode mediating these correlations. While this proof-of-principle experiment is realized on a vibrational mode in a bulk diamond crystal, the effect that is revealed should be universally observable in Raman-active molecules and solids. Our scheme for producing hybrid photon-phonon entanglement is agnostic to sample details and is passively phase-stabilized, while our two-color pump-probe technique can address Raman-active vibrations irrespective of any polarization selection rules—all of which differ from earlier work (*17*). Our results demonstrate the strongest form of quantum correlations and is thus a powerful generalization of techniques deployed in atomic physics to study the decoherence of entanglement (*27*).

MATERIALS AND METHODS

The inelastic scattering of light off an internal vibrational mode—vibrational Raman scattering—is analogous to the radiation-pressure interaction between light and a mechanically compliant mirror (*28*). Specifically, the Raman interaction consists of two processes. In the Stokes process, a quantum of vibrational energy $\hbar\Omega_v$ (a phonon) is created together with a quantum of electromagnetic energy $\hbar\omega_s$ (a Stokes photon); in the anti-Stokes process, a phonon is annihilated while an anti-Stokes photon is created at angular frequency ω_a. Energy conservation demands that $\omega_{s,a} \pm \Omega_v = \omega_{in}$, respectively, where ω_{in} is the frequency of the incoming photon.

In our experiment, a diamond sample—grown along the [100] direction by a high-pressure, high-temperature method, about 300 μm thick and polished on both faces along the (100) crystallographic plane—is excited with femtosecond pulses from a mode-locked laser through a pair of high numerical aperture objectives (NA = 0.8) (the effective length over which the Raman interaction takes place is of the order of 2 μm). Since the pulses are shorter than the coherence time of the Raman-active vibration, but longer than its oscillation period, there exists perfect time correlation between the generation (annihilation) of a vibrational excitation and the production of a Stokes (anti-Stokes) photon. In the following, we show how to

[1]Institue of Physics, Ecole Polytechnique Fédérale de Lausanne, CH-1015 Lausanne, Switzerland. [2]LIGO Laboratory, Massachusetts Institute of Technology, Cambridge, MA 02139, USA. [3]Department of Mechanical Engineering, Massachusetts Institute of Technology, Cambridge, MA 02139, USA. [4]Departement Physik, Universität Basel, Klingelbergstrasse 82, CH-4056 Basel, Switzerland. [5]Université Paris-Saclay, CEA, CNRS, Institut de physique théorique, 91191, Gif-sur-Yvette, France.
*Corresponding author. Email: chris.galland@epfl.ch (C.G.); nicolas.sangouard@unibas.ch (N.S.)

leverage this time correlation to generate time-bin entanglement (*29*) between two effective photonic qubits that reveal properties of the mediating phonon mode and quantify the strength of the quantum correlations using the Clauser-Horne-Shimony-Holt (CHSH) form of the Bell inequality (*4*).

The scheme (Fig. 1) starts when a pair of laser pulses, labeled "write" and "read," impinge on the sample. Each is a classical wave packet with $\sim10^8$ photons per pulse. Their central frequencies are independently tunable, which allows spectral filtering of the Stokes field generated by the write pulse and the anti-Stokes field generated by the read pulse. The delay between them, Δt, is adjustable to probe the decoherence of the vibrational mode. Each pulse passes through an unbalanced Mach-Zehnder interferometer and is split in two temporal modes separated by $\Delta T_{bin} \gg \Delta t$, which we label the "early" and "late" time bins. $\Delta T_{bin} \simeq 3$ ns is chosen to be much longer than the expected vibrational coherence time, which ensures that there can be no quantum-coherent interaction between the two time bins mediated by the vibrational mode.

At room temperature, the thermal state of the vibrational mode (*26*) (at 39.9 THz) has as a mean occupancy of 1.5×10^{-3}. The initial state of the vibration in the two time bins is therefore very well approximated by the ground state $|0_v\rangle \equiv |0_{v,E}\rangle \otimes |0_{v,L}\rangle$, where the subscripts E and L stand for the early and late time bins, respectively. The Stokes (*s*) and anti-Stokes (*a*) fields are also in the vacuum state at the start of the experiment, denoted by $|0_s\rangle \equiv |0_{s,E}\rangle \otimes |0_{s,L}\rangle$ and $|0_a\rangle \equiv |0_{a,E}\rangle \otimes |0_{a,L}\rangle$.

The interaction of the write pulse (split into the two time bins) with the vibrational mode generates a two-mode squeezed state of the Stokes and vibrational fields (*26*) in each time bin. A read pulse delayed by Δt (also split into the two time bins) maps the vibrational state in the respective time bins onto its anti-Stokes sideband.

Since we perform the experiment in the regime of very low Stokes scattering probability and postselect the outcomes where exactly one Stokes photon and one anti-Stokes photon were detected (see the Supplementary Materials for the treatment of triple coincidence), our scheme can be described in a subspace of the full Hilbert space that contains one vibrational excitation only, shared by the early and late time bin. We therefore introduce the shortened notation $|E_v\rangle \equiv \hat{v}_E^\dagger|0_v\rangle; |L_v\rangle \equiv \hat{v}_L^\dagger|0_v\rangle$ for the single phonon states (here, $\hat{v}^\dagger$ is the phonon creation operator), and $|E_s\rangle \equiv \hat{s}_E^\dagger|0_s\rangle; |L_s\rangle \equiv \hat{s}_L^\dagger|0_s\rangle$
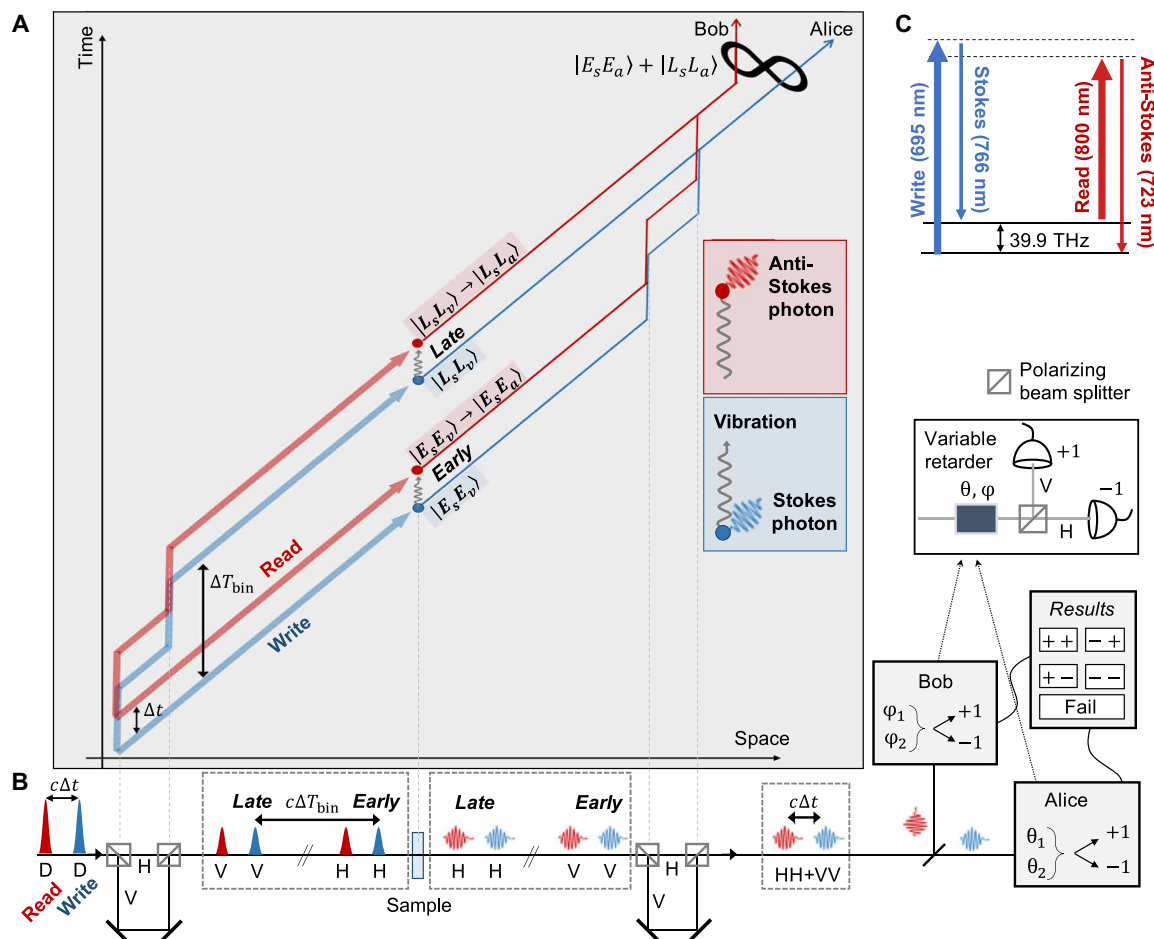

Fig. 1. Conceptual scheme and simplified experimental layout. (**A**) Space-time diagram representation of the time-bin entanglement procedure. (**B**) Corresponding experimental implementation unfolded in space along the horizontal axis (see section S1 for details). Contents of the dashed boxes illustrate the time sequence and polarization of the excitation pulses (Gaussian wave packets) and Raman-scattered photons (wavy arrows), during a single repetition of the experiment. The polarization states are denoted by D (diagonal), H (horizontal), and V (vertical). Note that, in our geometry, the polarization of Raman-scattered photons is orthogonal to that of the incoming pulses. The vertical dashed lines in (A) correspond to different points in space along the setup. (**C**) Energy diagram of the relevant Raman interactions, showing the center wavelengths used in the experiment.

for the Stokes single photon states (here, $\hat{s}^{\dagger}$ is the Stokes photon creation operator). Conditioned on the detection of a single Stokes photon, the hybrid light-vibrational state can be written in the basis $\{|E_s\rangle, |L_s\rangle\} \otimes \{|E_v\rangle, |L_v\rangle\} = \{|E_s, E_v\rangle, |E_s, L_v\rangle, |L_s, E_v\rangle, |L_s, L_v\rangle\}$. In this sense, we can speak of vibrational and photonic qubits encoded in the time bin basis.

Within each time bin, the read pulse implements (with a small probability ~0.1%) the map $|E_s, E_v\rangle \rightarrow |E_s, E_a\rangle$ and $|L_s, L_v\rangle \rightarrow |L_s, L_a\rangle$, where we have defined $|E_a\rangle \equiv \hat{a}_E^{\dagger}|0_a\rangle$ and $|L_a\rangle \equiv \hat{a}_L^{\dagger}|0_a\rangle$ (here, $\hat{a}_{E,L}^{\dagger}$ are the creation operators for the anti-Stokes photon in each time bin). Detection of an anti-Stokes photon in coincidence with a Stokes photon from the write pulse heralds that the time bin qubit was successfully mapped onto an anti-Stokes photonic qubit.

By passing the Stokes and anti-Stokes photons through an unbalanced interferometer identical to the one used on the excitation path (Fig. 1B and the Supplementary Materials), "which-time" information is erased. Moreover, the use of polarizing beam splitters in the interferometer maps the time bin–encoded Stokes and anti-Stokes photonic qubits onto polarization-encoded qubits after they are temporally overlapped, $|E_s, E_a\rangle \rightarrow |V_s, V_a\rangle$ and $|L_s, L_a\rangle \rightarrow |H_s, H_a\rangle$, where H and V refer to two orthogonal polarizations of the same temporal mode. We thus prepare the heralded Bell correlated state

$$|\psi_{s,a}\rangle = \frac{1}{\sqrt{2}}(|V_s, V_a\rangle - e^{i\phi}|H_s, H_a\rangle) \qquad (1)$$

where the phase ϕ is the sum of the phases acquired by the Stokes and anti-Stokes photons coming from the late time bin, with respect to the early time bin (the apparatus is set to realize $\phi = 0$). As detailed in fig. S1, the experiment is passively phase-stable by design.

To prove Bell correlations mediated by the room temperature macroscopic vibration, we send the Stokes and anti-Stokes signals to two independent measurement apparatus labeled Alice and Bob, respectively, who perform local rotations of the Stokes and anti-Stokes states before making a projective measurement in the two-dimensional basis $\{|V_s\rangle, |H_s\rangle\}$ and $\{|V_a\rangle, |H_a\rangle\}$, respectively. Each party will obtain one of two outcomes, which we label "+" or "−". The number of coincident events where Alice obtains the outcome $x \in \{+, -\}$ and Bob obtains the outcome $y \in \{+, -\}$ is denoted n_{xy}. We then define the normalized correlation parameter

$$E_{\theta, \varphi} = \frac{n_{++} + n_{--} - n_{+-} - n_{-+}}{n_{++} + n_{--} + n_{+-} + n_{-+}} \qquad (2)$$

where the angles θ and φ label the rotations that Alice and Bob, respectively, perform on their qubits before the measurement. It is defined in such a way that fully correlated events for a given pair of rotation angles $\{\theta, \varphi\}$ yield $E_{\theta, \varphi} = 1$ while perfectly anticorrelated events yield $E_{\theta, \varphi} = -1$. The CHSH parameter (2)

$$S = E_{\theta_1, \varphi_1} + E_{\theta_2, \varphi_2} + E_{\theta_1, \varphi_2} - E_{\theta_2, \varphi_1} \qquad (3)$$

certifies Bell correlations when $|S| > 2$. In particular, for our scenario, where we target the Bell correlated state (Eq. 1), a maximal violation is expected for $\{\theta_1, \theta_2\} = \{0, \frac{\pi}{2}\}$ and $\{\varphi_1, \varphi_2\} = \{-\frac{\pi}{4}, \frac{\pi}{4}\}$.

RESULTS
Observation of Bell correlations
Figure 2 shows the CHSH parameter (Eq. 3) measured for a varying write-read delay. Our data demonstrate a clear violation of the Bell
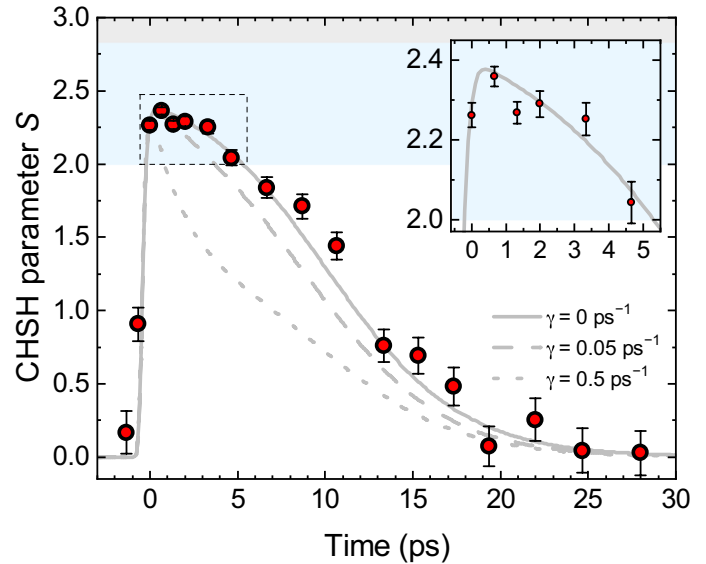

Fig. 2. Time-resolved photon-phonon Bell correlations. The CHSH parameter S (Eq. 3) as a function of write-read delay Δt, with a zoom near $\Delta t = 0$ as an inset. Full circles are experimental data, while error bars are computed from a Monte Carlo simulation (see section S2 for details). The solid gray line is obtained from the model with zero pure dephasing and no other free parameters, while dashed lines illustrate the impact of two different nonzero values. The blue region, demarcated by $2 < |S| \leq 2\sqrt{2}$, certifies Bell correlations, while the gray region above it is forbidden for nonsuperluminal theories.

inequality (whose classical bound is marked as the white region) that persists for more than 5 ps, about 50 times longer that the write and read pulse duration. While this time scale is consistent with the phonon lifetime in diamond, the dynamics of Bell correlations in fact strongly depends on experimental noise and nonidealities, as explained in sections S4 to S6. At a time delay of 0.66 ps, for which there is vanishing temporal overlap of the write and read pulses within the sample and correlations are only mediated by the vibration, we measure $S = 2.360 \pm 0.025$. This confirms Bell correlations mediated by the vibration that acts as a room temperature quantum memory (30–34).

A detailed analysis of the event statistics (see section S6) enables us to make a more precise claim concerning the violation of the Bell inequality (35), without assuming that our data are independent and identically distributed. From this analysis, we can claim with a confidence level of 1×10^{-7} to 6×10^{-7} that the postselected Stokes–anti-Stokes state features Bell correlations with a minimum value of the CHSH parameter $S_{\min} = 2.23$.

Note that we rely on the fair sampling assumption (36) since the overall detection efficiency in our experiment is not high enough to test a Bell inequality without postselection of events where at least one detector clicks on each side (Alice and Bob). However, it can be shown (37) that when all detectors are equally efficient—a condition well approximated in our experiment—the postselected data are faithful to that from an ideal experiment where lossless devices measure a state obtained by quantum filtering the actual Stokes–anti-Stokes state. By reporting a CHSH value higher than 2, we show that this filtered state is Bell correlated.

To gain further insight into the nature of the Bell correlated state prepared in the experiment, and the reasons why the quantum bound ($|S| = 2\sqrt{2}$) is not saturated, we perform further measurements. Figure 3A shows the one-photon counts as Bob's analysis angle is
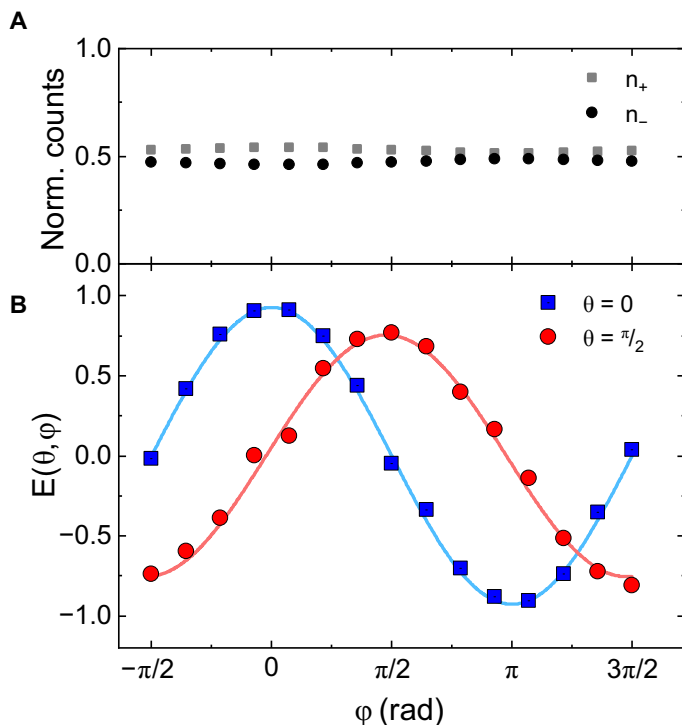
Fig. 3. Phonon-mediated two-photon interference. (**A**) Normalized single-photon count rates on the two anti-Stokes detectors as a function of Bob's rotation angle φ. The ideal marginal state is the statistical mixture $p|E_a\rangle\langle E_a| - (1-p)|L_a\rangle \langle L_a|$, with $p = \frac{1}{2}$; data are consistent with $|p - \frac{1}{2}| = 0.027$. Error bars are several times smaller than symbol size. (**B**) Two-photon interferences in the Stokes–anti-Stokes coincidence rate as a function of Bob's rotation angle φ. The normalized correlation parameter $E(\theta; \varphi)$ (Eq. 2) is plotted for two fixed angles $\theta = 0$ (blue squares) and $\theta = \pi/2$ (red circles) for Alice's rotation on the Stokes state, at a fixed write-read delay of $t = 0.66$ ps. Experimental data are represented by full symbols (error bars are smaller than symbol size); solid lines are fitting curves to extract the visibility (see the Supplementary Materials for details).

rotated. For an ideal Bell state, the marginal state is maximally mixed and should lead to no dependence of the one-photon counts on the analysis angle. The observed data are consistent with a deviation from a maximal mixture by 2.7%.

Figure 3B shows two-photon interference for various settings of Bob's measurement angle for two fixed values of Alice's measurement angle, $\theta = 0, \pi/2$, and a fixed write-read delay of 0.66 ps. The interference is consistent with a model (see section S3) where the Stokes interaction creates a two-mode light-vibration squeezed state and that anti-Stokes scattering implements a beam splitter interaction (26).

The curve for the setting $\theta = 0$ (Fig. 3B, blue trace) reveals how accurately we can prepare and distinguish the two states $|E_s, E_a\rangle$ and $|L_s, L_a\rangle$. At a given delay, the visibility has an upper limit related to the strength of Stokes–anti-Stokes photon number correlations, $V_{\max} = \frac{g_{s,a}^{(2)} - 1}{g_{s,a}^{(2)} + 1}$ (27), where $g_{s,a}^{(2)}$ is the normalized second-order cross-correlation (22) (see the Supplementary Materials). The value extracted from the fit is $V_{\theta=0} = 93 \pm 1\%$, in agreement with the independently measured value of $g_{s,a}^{(2)}(0) = 25$, showing that the signal-to-noise ratio in the cross-correlation is indeed the limiting factor for the visibility in this setting. This visibility could be improved by reducing the power of the write beam (to decrease the probability of creating multiple Stokes-phonon pairs in one pulse) and that of the

read beam (to reduce the noise from degenerate four-wave mixing). Note that because of the small interaction length ($\sim$2 μm), phase matching is not a relevant concern.

The coincidence curve for $\theta = \frac{\pi}{2}$ (Fig. 3B, red trace) corresponds to a rotated measurement basis for Alice and is sensitive to the fluctuations of the phase ϕ in the superposition of Eq. 1. To accommodate this possibility, we model the relative phase ϕ in Eq. 1 to be distributed as a zero-mean Gaussian random variable with variance σ (see the Supplementary Materials). We extract a visibility $V_{\theta=\pi/2} = 76\%$ from the fit to the experimental data, which is reproduced by the model for a standard deviation $\sigma = 0.31$ rad (equivalent to a $\pm$0.18 fs timing uncertainty maintained over $\sim$4 min). Ultimately, we are able to predict all measured quantities from independently characterized parameters, namely, the Raman scattering probability, the overall Raman signal detection efficiency, and the dark count rate of the detectors (see section S4).

Decoherence dynamics of the phonon mode
From the temporal behavior of the CHSH parameter, we can extract the rate of pure dephasing of the vibrational mode mediating the Bell correlations. In the absence of pure dephasing, the CHSH parameter decays with the collective vibrational mode. Pure dephasing, in contrast, scrambles the phase ϕ of the superposition in state (Eq. 1). We model it as a random walk of the phase at the characteristic time scale γ^{-1}, so that the standard deviation of the phase ϕ increases with the write-read delay (in addition to technical fluctuations) as $\sigma = \sqrt{\gamma\, \Delta t}$ (see section S3.6). The model is plotted against the data of Fig. 2 (solid line), and the best agreement with the data is obtained with a pure dephasing rate identically null (other pure dephasing rates are plotted for comparison), consistent with previous measurements of the coherence time of a single vibrational mode in diamond using transient coherent ultrafast phonon spectroscopy (38).

DISCUSSION
We have produced Bell correlations between two photons through their interaction with a common Raman-active phonon at room temperature and probed their decay with sub-picosecond resolution. Our data show that Bell correlations are preserved for more than 200 oscillation periods at room temperature, evidencing a mechanical coherence time at par with the state of the art for microfabricated resonators under high vaccum (39). Optical phonons in diamond indeed exhibit a room temperature "Q-frequency product" of $\sim$4 $\times$ 10^{16} Hz, making them attractive resonators for ultrafast quantum technologies.

Such highly coherent vibrational modes, together with the toolset of time-resolved single photon Raman spectroscopy that we have demonstrated here, should allow one to entangle two vibrational qubits via entanglement swapping (40) or to perform optomechanical conversion between photonic qubits at different frequencies (41), among other possible applications. Much longer vibrational coherence times could be achieved with ensembles of molecules that are decoupled from the phonon bath by surface engineering (42) or optical trapping and cooling (43). Besides, molecules in the gas phase exhibit more complex mechanical degrees of freedom, including rotational and rovibrational modes (44), with increased coherence time and rich opportunities for quantum information processing (45). In the future, our scheme could be applied to individual molecules free of heterogeneous broadening using the enhancement

of light-vibration coupling offered by electronic resonances (*46*), plasmonic nanocavities (*47*), or optical microcavities (*48*).

In addition to being a benchmark for the robust generation of optomechanical Bell correlations at room temperature, our work suggests a new class of techniques able to probe the role of phonon-mediated entanglement in quantum technologies (*49*), chemistry (*50*), or even biology (*51*).

SUPPLEMENTARY MATERIALS

Supplementary material for this article is available at http://advances.sciencemag.org/cgi/content/full/6/51/eabb0260/DC1

REFERENCES AND NOTES

1. J. S. Bell, On the Einstein Podolsky Rosen paradox. *Physics* **1**, 195–200 (1964).
2. J. F. Clauser, M. A. Horne, A. Shimony, R. A. Holt, Proposed experiment to test local hidden-variable theories. *Phys. Rev. Lett.* **23**, 880 (1969).
3. N. Brunner, D. Cavalcanti, S. Pironio, V. Scarani, S. Wehner, Bell nonlocality. *Rev. Mod. Phys.* **86**, 419 (2014).
4. S. J. Freedman, J. F. Clauser, Experimental test of local hidden-variable theories. *Phys. Rev. Lett.* **28**, 938 (1972).
5. A. Aspect, P. Grangier, G. Roger, Experimental tests of realistic local theories via Bell's theorem. *Phys. Rev. Lett.* **47**, 460 (1981).
6. C.-W. Chou, J. Laurat, H. Deng, K. S. Choi, H. de Riedmatten, D. Felinto, H. J. Kimble, Functional quantum nodes for entanglement distribution over scalable quantum networks. *Science* **316**, 1316–1320 (2007).
7. J. Hofmann, M. Krug, N. Ortegel, L. Gérard, M. Weber, W. Rosenfeld, H. Weinfurter, Heralded entanglement betweenwidely separated atoms. *Science* **337**, 72–75 (2012).
8. R. Blatt, D. Wineland, Entangled states of trapped atomic ions. *Nature* **453**, 1008–1015 (2008).
9. D. N. Matsukevich, T. Chaneliére, M. Bhattacharya, S.-Y. Lan, S. D. Jenkins, T. A. B. Kennedy, A. Kuzmich, Entanglement of a photon and a collective atomic excitation. *Phys. Rev. Lett.* **95**, 040405 (2005).
10. L. Li, Y. O. Dudin, A. Kuzmich, Entanglement between light and an optical atomic excitation. *Nature* **498**, 466–469 (2013).
11. N. J. Engelsen, R. Krishnakumar, O. Hosten, M. A. Kasevich, Bell correlations in spinsqueezed states of 500 000 atoms. *Phys. Rev. Lett.* **118**, 140401 (2017).
12. M. Ansmann, H. Wang, R. C. Bialczak, M. Hofheinz, E. Lucero, M. Neeley, A. D. O'Connell, D. Sank, M. Weides, J. Wenner, A. N. Cleland, J. M. Martinis, Violation of Bell's inequality in Josephson phase qubits. *Nature* **461**, 504–506 (2009).
13. L. DiCarlo, M. D. Reed, L. Sun, B. R. Johnson, J. M. Chow, J. M. Gambetta, L. Frunzio, S. M. Girvin, M. H. Devoret, R. J. Schoelkopf, Preparation and measurement of three-qubit entanglement in a superconducting circuit. *Nature* **467**, 574–578 (2010).
14. J. P. Dehollain, S. Simmons, J. T. Muhonen, R. Kalra, A. Laucht, F. Hudson, K. M. Itoh, D. N. Jamieson, J. C. McCallum, A. S. Dzurak, A. Morello, Bell's inequality violation with spins in silicon. *Nat. Nanotechnol.* **11**, 242–246 (2016).
15. B. Hensen, H. Bernien, A. E. Dréau, A. Reiserer, N. Kalb, M. S. Blok, J. Ruitenberg, R. F. L. Vermeulen, R. N. Schouten, C. Abellán, W. Amaya, V. Pruneri, M. W. Mitchell, M. Markham, D. J. Twitchen, D. Elkouss, S. Wehner, T. H. Taminiau, R. Hanson, Loophole-free bell inequality violation using electron spins separated by 1.3 kilometres. *Nature* **526**, 682–686 (2015).
16. I. Marinković, A. Wallucks, R. Riedinger, S. Hong, M. Aspelmeyer, S. Gröblacher, Optomechanical bell test. *Phys. Rev. Lett.* **121**, 220404 (2018).
17. K. C. Lee, M. R. Sprague, B. J. Sussman, J. Nunn, N. K. Langford, X.-M. Jin, T. Champion, P. Michelberger, K. F. Reim, D. England, D. Jaksch, I. A. Walmsley, Entangling macroscopic diamonds at room temperature. *Science* **334**, 1253–1256 (2011).
18. A. Jorio, M. Kasperczyk, N. Clark, E. Neu, P. Maletinsky, A. Vijayaraghavan, L. Novotny, Stokes and anti-Stokes Raman spectra of the high-energy C–C stretching modes in graphene and diamond. *Phys. Status Solidi B* **252**, 2380–2384 (2015).
19. M. Kasperczyk, A. Jorio, E. Neu, P. Maletinsky, L. Novotny, Stokes–anti-Stokes correlations in diamond. *Opt. Lett.* **40**, 2393–2396 (2015).
20. D. G. England, K. A. G. Fisher, J.-P. W. MacLean, P. J. Bustard, K. Heshami, K. J. Resch, B. J. Sussman, Phonon-mediated nonclassical interference in diamond. *Phys. Rev. Lett.* **117**, 073603 (2016).
21. P.-Y. Hou, Y.-Y. Huang, X.-X. Yuan, X.-Y. Chang, C. Zu, L. He, L.-M. Duan, Quantum teleportation from light beams to vibrational states of a macroscopic diamond. *Nat. Commun.* **7**, 11736 (2016).
22. M. D. Anderson, S. T. Velez, K. Seibold, H. Flayac, V. Savona, N. Sangouard, C. Galland, Two-color pump-probe measurement of photonic quantum correlations mediated by a single phonon. *Phys. Rev. Lett.* **120**, 233601 (2018).
23. P. J. Bustard, J. Erskine, D. G. England, J. Nunn, P. Hockett, R. Lausten, M. Spanner, B. J. Sussman, Nonclassical correlations between terahertz-bandwidth photons mediated by rotational quanta in hydrogen molecules. *Opt. Lett.* **40**, 922–925 (2015).
24. M. Kasperczyk, F. S. de Aguiar Júnior, C. Rabelo, A. Saraiva, M. F. Santos, L. Novotny, A. Jorio, Temporal quantum correlations in inelastic light scattering from water. *Phys. Rev. Lett.* **117**, 243603 (2016).
25. A. Saraiva, F. S. de Aguiar Júnior, R. de Melo e Souza, A. P. Pena, C. H. Monken, M. F. Santos, B. Koiller, A. Jorio, Photonic counterparts of cooper pairs. *Phys. Rev. Lett.* **119**, 193603 (2017).
26. S. T. Velez, K. Seibold, N. Kipfer, M. D. Anderson, V. Sudhir, C. Galland, Preparation and decay of a single quantum of vibration at ambient conditions. *Phys. Rev. X* **9**, 041007 (2019).
27. H. de Riedmatten, J. Laurat, C. W. Chou, E. W. Schomburg, D. Felinto, H. J. Kimble, Direct measurement of decoherence for entanglement between a photon and stored atomic excitation. *Phys. Rev. Lett.* **97**, 113603 (2006).
28. P. Roelli, C. Galland, N. Piro, T. J. Kippenberg, Molecular cavity optomechanics as a theory of plasmon-enhanced raman scattering. *Nat. Nanotechnol.* **11**, 164–169 (2016).
29. I. Marcikic, H. de Riedmatten, W. Tittel, V. Scarani, H. Zbinden, N. Gisin, Time-bin entangled qubits for quantum communication created by femtosecond pulses. *Phys. Rev. A* **66**, 062308 (2002).
30. D. G. England, P. J. Bustard, J. Nunn, R. Lausten, B. J. Sussman, From photons to phonons and back: A THz optical memory in diamond. *Phys. Rev. Lett.* **111**, 243601 (2013).
31. D. G. England, K. A. G. Fisher, J.-P. W. MacLean, P. J. Bustard, R. Lausten, K. J. Resch, B. J. Sussman, Storage and retrieval of THz-bandwidth single photons using a room-temperature diamond quantum memory. *Phys. Rev. Lett.* **114**, 053602 (2015).
32. K. A. G. Fisher, D. G. England, J.-P. W. MacLean, P. J. Bustard, K. J. Resch, B. J. Sussman, Frequency and bandwidth conversion of single photons in a room-temperature diamond quantum memory. *Nat. Commun.* **7**, 11200 (2016).
33. P. J. Bustard, D. G. England, K. Heshami, C. Kupchak, B. J. Sussman, Quantum frequency conversion with ultra-broadband tuning in a Raman memory. *Phys. Rev. A* **95**, 053816 (2017).
34. K. A. G. Fisher, D. G. England, J.-P. W. MacLean, P. J. Bustard, K. Heshami, K. J. Resch, B. J. Sussman, Storage of polarization-entangled THz-bandwidth photons in a diamond quantum memory. *Phys. Rev. A* **96**, 012324 (2017).
35. J.-D. Bancal, K. Redeker, P. Sekatski, W. Rosenfeld, N. Sangouard, Device-independent certification of an elementary quantum network link. (2018).
36. D. W. Berry, H. Jeong, M. Stobińska, T. C. Ralph, Fair-sampling assumption is not necessary for testing local realism. *Phys. Rev. A* **81**, 012109 (2010).
37. D. Orsucci, J.-D. Bancal, N. Sangouard, P. Sekatski, How post-selection affects device-independent claims under the fair sampling assumption. *Quantum* **4**, 238 (2020).
38. F. C. Waldermann, B. J. Sussman, J. Nunn, V. O. Lorenz, K. C. Lee, K. Surmacz, K. H. Lee, D. Jaksch, I. A. Walmsley, P. Spizziri, P. Olivero, S. Prawer, Measuring phonon dephasing with ultrafast pulses using raman spectral interference. *Phys. Rev. B* **78**, 155201 (2008).
39. A. H. Ghadimi, S. A. Fedorov, N. J. Engelsen, M. J. Bereyhi, R. Schilling, D. J. Wilson, T. J. Kippenberg, Elastic strain engineering for ultralow mechanical dissipation. *Science* **360**, 764–768 (2018).
40. M. Żukowski, A. Zeilinger, M. A. Horne, A. K. Ekert, "Event-ready-detectors" Bell experiment via entanglement swapping. *Phys. Rev. Lett.* **71**, 4287 (1993).
41. J. T. Hill, A. H. Safavi-Naeini, J. Chan, O. Painter, Coherent optical wavelength conversion via cavity optomechanics. *Nat. Commun.* **3**, 1196 (2012).
42. L. Chen, J. A. Lau, D. Schwarzer, J. Meyer, V. B. Verma, A. M. Wodtke, The Sommerfeld ground-wave limit for a molecule adsorbed at a surface. *Science* **363**, 158–161 (2019).
43. S. S. Kondov, C.-H. Lee, K. H. Leung, C. Liedl, I. Majewska, R. Moszynski, T. Zelevinsky, Molecular lattice clock with long vibrational coherence. *Nat. Phys.* **15**, 1118–1122 (2019).
44. C. P. Koch, M. Lemeshko, D. Sugny, Quantum control of molecular rotation. *Rev. Mod. Phys.* **91**, 035005 (2019).
45. V. V. Albert, J. P. Covey, J. Preskill, Robust encoding of a qubit in a molecule. *Phys. Rev. X* **10**, 031050 (2020).
46. A. Maser, B. Gmeiner, T. Utikal, S. Götzinger, V. Sandoghdar, Few-photon coherent nonlinear optics with a single molecule. *Nat. Photonics* **10**, 450–453 (2016).
47. S. Yampolsky, D. A. Fishman, S. Dey, E. Hulkko, M. Banik, E. O. Potma, V. A. Apkarian, Seeing a single molecule vibrate through time-resolved coherent anti-Stokes Raman scattering. *Nat. Photonics* **8**, 650–656 (2014).
48. D. Riedel, S. Flågan, P. Maletinsky, R. J. Warburton, Cavity-enhanced raman scattering for *in situ* alignment and characterization of solid-state microcavities. *Phys. Rev. Applied* **13**, 014036 (2020).
49. M. Aspelmeyer, T. J. Kippenberg, F. Marquardt, Cavity optomechanics. *Rev. Mod. Phys.* **86**, 1391 (2014).
50. A. Halpin, P. J. M. Johnson, R. Tempelaar, R. S. Murphy, T. L. C. Jansen, R. J. D. Miller, Two-dimensional spectroscopy of a molecular dimer unveils the effects of vibronic coupling on exciton coherences. *Nat. Chem.* **6**, 196–201 (2014).

51. H.-G. Duan, V. I. Prokhorenko, R. J. Cogdell, K. Ashraf, A. L. Stevens, M. Thorwart, R. J. D. Miller, Nature does not rely on long-lived electronic quantum coherence for photosynthetic energy transfer. *Proc. Natl. Acad. Sci. U.S.A.* **114**, 8493–8498 (2017).

52. X. Chen, X. Lu, S. Dubey, Q. Yao, S. Liu, X. Wang, Q. Xiong, L. Zhang, A. Srivastava, Entanglement of single-photons and chiral phonons in atomically thin WSe₂. *Nat. Phys.* **15**, 221–227 (2019).

53. P. Sekatski, N. Sangouard, F. Bussières, C. Clausen, N. Gisin, H. Zbinden, Detector imperfections in photon-pair source characterization. *J. Phys. B At. Mol. Opt. Phys.* **45**, 124016 (2012).

Citation: S. Tarrago Velez, V. Sudhir, N. Sangouard, C. Galland, Bell correlations between light and vibration at ambient conditions. *Sci. Adv.* **6**, eabb0260 (2020).

ScienceAdvances

Bell correlations between light and vibration at ambient conditions

Santiago Tarrago VelezVivishek SudhirNicolas SangouardChristophe Galland

View the article online
https://www.science.org/doi/10.1126/sciadv.abb0260
Permissions
https://www.science.org/help/reprints-and-permissions

Use of think article is subject to the Terms of service